SCIENCE CHINA
Earth Sciences

• RESEARCH PAPER •

March 2013 Vol.56 No.3: 354–365
doi: 10.1007/s11430-012-4514-0

Late Quaternary glacial chronology on the eastern slope of Gongga Mountain, eastern Tibetan Plateau, China

WANG Jie*, PAN BaoTian, ZHANG GuoLiang, CUI Hang, CAO Bo & GENG HaoPeng

Key Laboratory of Western China's Environmental Systems (Ministry of Education), Lanzhou University, Lanzhou 730000, China

Received February 21, 2012; accepted August 4, 2012; published online November 8, 2012

The Gongga Mountain is the largest area of modern glaciation in the Hengduan Mountains and, with a summit elevation of 7556 m, is the highest mountain on the eastern margin of the Tibetan Plateau. During the Quaternary glacial-interglacial cycles the Gongga Mountain was extensively and repeatedly glaciated, and glacial landforms and outwash deposits from multiple glaciations are well-preserved in valleys, in basins, and on piedmonts. To constrain the glacial chronology of the eastern slope of Gongga Mountain, sample sites were selected based on the distribution and weathering of glacial tills, relationships among glacial deposits, and soil development on moraines. Dating of the tills and glaciofluvial deposits was undertaken with electron spin resonance (ESR) and optically stimulated luminescence (OSL). The ages of the glacial deposits can be divided into four clusters: 2.2±0.5, 11.9±0.6, 35.9±2.7–58.0±6.3 and 119.2±15.9–194.2±32.8 ka. Five glacial advances in this region have been identified, which are equivalent in age to the Little Ice Age (LIA), Neoglaciation, marine oxygen isotope stage (MIS) 2, mid-MIS3, and MIS6. The largest local last glacial maximum (LGM_L) occurred on Gongga Mountain during mid-MIS3, characterized by a cold-humid climate, rather than the global Last Glacial Maximum (LGM_G) of MIS2. The Gongga, Nanmenguangou (NMGG) and Yajiageng Glaciations occurred during the late part of the last glacial cycle, the middle of the last glacial cycle and the penultimate glacial cycle, respectively. On the basis of geomorphological, sedimentological, and compositional characteristics, landforms of the Moxi Platform and terraces can be grouped by facies and geochronology. In combination with the dating results, this analysis indicates the basal part of the Moxi Platform between Xinxin and the Moxi Hotel is correlative with the till of the Nanguanmen Glaciation (mid-MIS3). This basal unit has occasional lenses of glaciofluvial sandy gravel and lacustrine sediments. The remainder of the Moxi Platform and the terraces beside the platform are glaciofluvial deposits occasionally mixed with debris flow deposits and range in age from MIS3 to Holocene.

ESR dating, glacial chronology, Gongga Mountain, Moxi Platform, OSL dating

Citation: Wang J, Pan B T, Zhang G L, et al. Late Quaternary glacial chronology on the eastern slope of Gongga Mountain, eastern Tibetan Plateau, China. Science China: Earth Sciences, 2013, 56: 354–365, doi: 10.1007/s11430-012-4514-0

The Tibetan Plateau and its bordering mountains have undergone intense tectonic uplift, which has been associated with river downcutting. Therefore, if preserved, older glacial landforms should be present at relatively higher elevations (i.e. platform, watershed and replat), and thus it is possible that the glacial landforms from the multiple glaciations are well-preserved. Studies of these landforms could provide essential information for reconstructing the sequences and history of Quaternary glaciations. It is believed that the initiation of glaciation in these regions is a result of the relationship of the timing of global ice ages and uplift of the Tibetan Plateau [1, 2]. Consequently, various air circulations, and the timing, rate and magnitude of uplift between different regions could result in the asynchronicity of the style and nature of Quaternary glaciations. In past decades, dating techniques have been refined and applied widely,

*Corresponding author (email: wangjie@lzu.edu.cn)

which can potentially determine the absolute ages of glacial landforms and sediments. Many scholars have applied one or several techniques to determine the timing of the Quaternary glacial landforms in some regions [3–11]. These studies have provided insights into the comparison of the timing of glaciations between different regions, and to simulate the evolution of glacial geomorphology and to reconstruct the paleo-environment. In tectonically active regions, these studies also can potentially provide information on the history of uplift.

Gongga Mountain covers the middle of the Daxue Mountain Range on the eastern margin of the Tibetan Plateau, and is geomorphologically located in a transitional region between the Sichuan Basin and the Tibetan Plateau. This region has experienced intense neotectonic movement since the Quaternary. Gongga Mountain, which stretches in a north-south direction, is the largest area of modern glaciation in the Hengduan Mountains. These glaciers experienced large advances and retreats during the glacial-interglacial cycles of the Quaternary, and the glacial landforms, especially the deposited landforms from multiple glaciations, are well-preserved in the valley, in the basin, and on the piedmont. Previous studies have included geomorphological mapping, some ^{14}C dates of wood buried within the moraines, terrestrial cosmogenic nuclide (TCN) ^{10}Be surface exposure ages of the moraines in the Hailuogou (HLG) valley and the glaciolfluvial deposits of the Moxi Platform [12–23]. Although significant work on the Quaternary glacial landforms and moraines in Gongga Mountain has been completed, contention still exists regarding the timing and extent of the glaciations due to the limited studies on glacial chronology, especially for the moraines older than the late part of last glacial cycle corresponding to the marine oxygen isotope stages (MIS) 2.

To reconstruct the timing of the multiple glaciations in this region, we studied the glacial landform and outwash deposits on the eastern slope of Gongga Mountain, by undertaking remote sensing, field mapping, geomorphological and sedimentological analysis, and numerical dating (including electron spin resonance (ESR) and optically simulated luminescence (OSL)). Based on the principles of geomorphology and stratigraphy, and the available dates, we discuss the style of Quaternary glaciations in this region.

1 Study area

There are 28 peaks above 6000 m a.s.l. in the Gongga Mountain (29°20′–30°20′N, 101°30′–102°15′E), with the highest peak at 7556 m a.s.l. The area higher than 5000 m a.s.l. accounts for approximately 1/6 of the total mountain [24] (Figure 1). The geomorphology of this region is characterized by high mountains and deep valleys. For example, the relative height from the Dadu River to the Gongga Peak reaches 6500 m, over a horizontal distance of 29 km. The Gongga Mountain is climatically dominated by the south Asian monsoon, the east Asian monsoon and the mid-latitude westerlies, and located in a transition region between the warm-wet monsoon climatic area of the eastern subtropics and cold-dry area of the Tibetan Plateau [20]. At HLG Station (29.573°N, 101.992°E, 3000 m a.s.l.) on the eastern slope of Gongga Mountain, the mean annual temperature was 4.1°C and the mean annual precipitation was 1,691 mm during the period 1988–2005. More than 80% of the annual precipitation occurs between May and August.

The 74 typical monsoon temperate glaciers with a total area of 257.66 km^2 are distributed in this region [25], and contain five valley glaciers longer than 10 km (Table 1), including HLG Glacier, Mozigou (MZG) Glacier, Yanzigou (YZG) Glacier, Nanmenguangou (NMGG) Glacier on the eastern slope and Dagongba (DGB) Glacier on the western slope (Figure 1). The present equilibrium line altitudes (ELAs) range from 4800 to 5000 m a.s.l. on the eastern slope of Gongga Mountain, and from 5000 to 5200 m a.s.l. on the western slope [26]. The mean annual temperature is −4.4°C on the eastern slope, and −4.1 to −5°C on the western slope. The mean annual precipitation at present ELAs is 3000 mm on the eastern slope and only 1800 mm on the western slope [26].

2 Quaternary glacial and glaciofluvial sediments on the eastern slope of Gongga Mountain

2.1 Glacial sediments

On the eastern slope of Gongga Mountain, there are 33 modern glaciers covering an area of 155.10 km^2, which is

Table 1 Parameters of valley glaciers with lengths >10 km in Gongga Mountain [25]

Glacier names and Nos.	Length (km)	Width (km)	Orientation of ablation area	Area (km^2)	Ice volume (km^3)	Top altitude (m a.s.l.)	Terminus (m a.s.l.)	ELA (m a.s.l.)
HLG (5K612F–3)	13.1	2.0	SE	25.71	3.3423	7556	2980	4880
MZG (5K612F–8)	11.6	2.3	NE	26.76	3.5056	6886	3600	5240
YZG (5K612F–13)	10.5	3.1	NE	32.15	4.4689	7556	3680	4840
NMGG (5K612F–25)	10.0	1.7	E	16.71	1.8882	6540	3460	4920
DGB (5K612D–44)	11.0	1.8	W	20.21	2.4252	6684	3660	4880

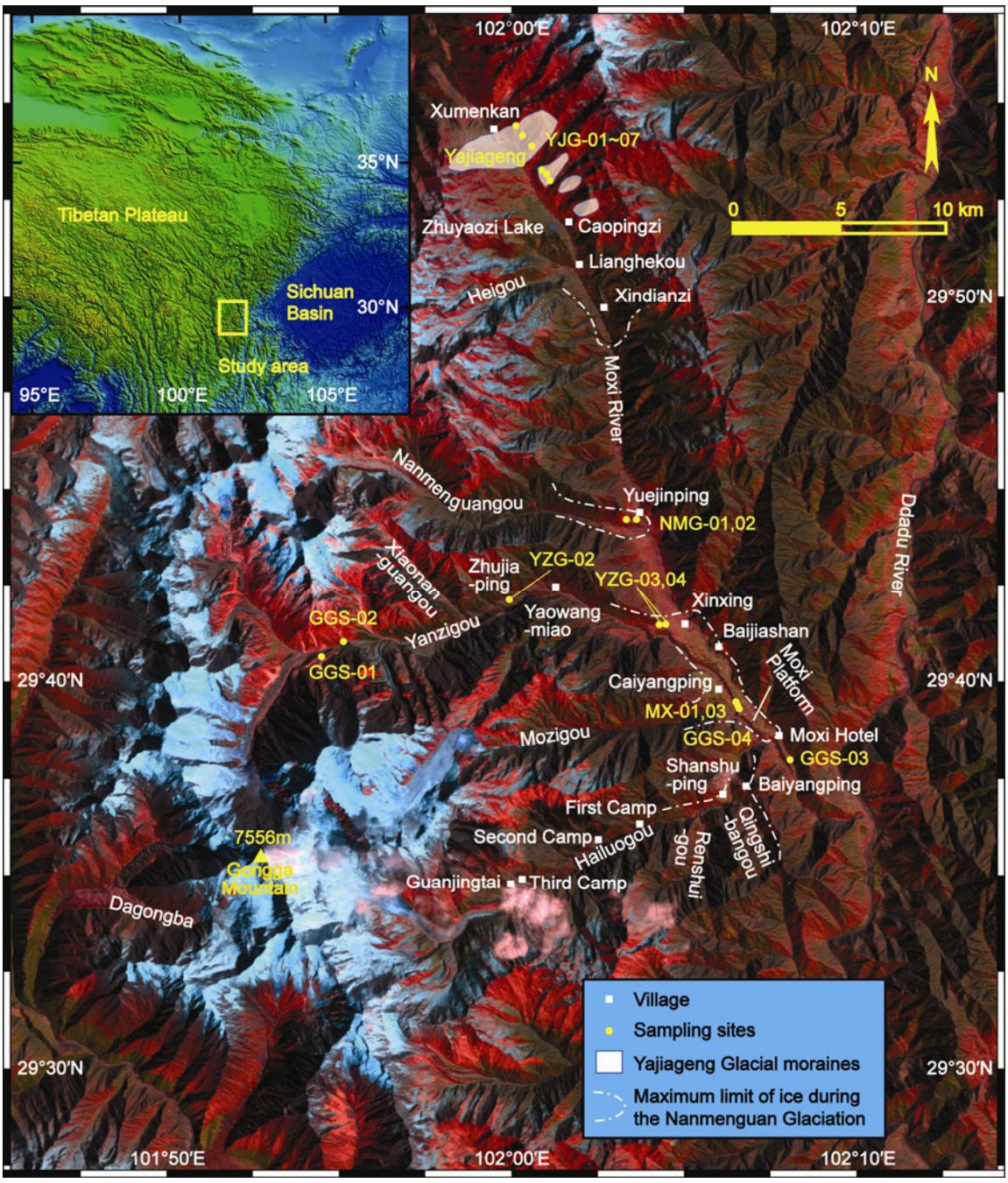

Figure 1 Landsat TM (Thematic Mapper) image and the sample's location in the Gongga Mountain region.

larger than those in the western region [25]. Four glaciers have lengths >10 km. Five distinctive sets of well-preserved moraines and associated glacial sediments are present from the terminus of the modern glacier to the Moxi Platform (Figure 2); therefore, this is an ideal region to reconstruct paleoglaciation.

The first set of moraines is typically located between several hundred meters and 3 km from the terminus of the modern glaciers and consists of several moraine ridges [20]. For example, three end moraines are preserved between the terminus of the HLG Glacier and the Dayanwo (Figure 3). The inner ridge, which rises approximately 30 m above the valley floor, is distributed at approximately 2850 m a.s.l. The outer ridge is distributed at a height approximately 50–100 m above the valley floor, with an altitude of 2800 m a.s.l. The middle ridge usually overlaps with the outer. Consequently, it is difficult to divide it from the outer ridge.

The second set of moraines is usually distributed on the outer flank of the first set of moraines and extends slightly down valley. This moraine set is well-preserved in the HLG and YZG valleys. Three moraine ridges are distributed at altitudes of 2750–3300 m a.s.l. near Guanjingtai (Figure 3).

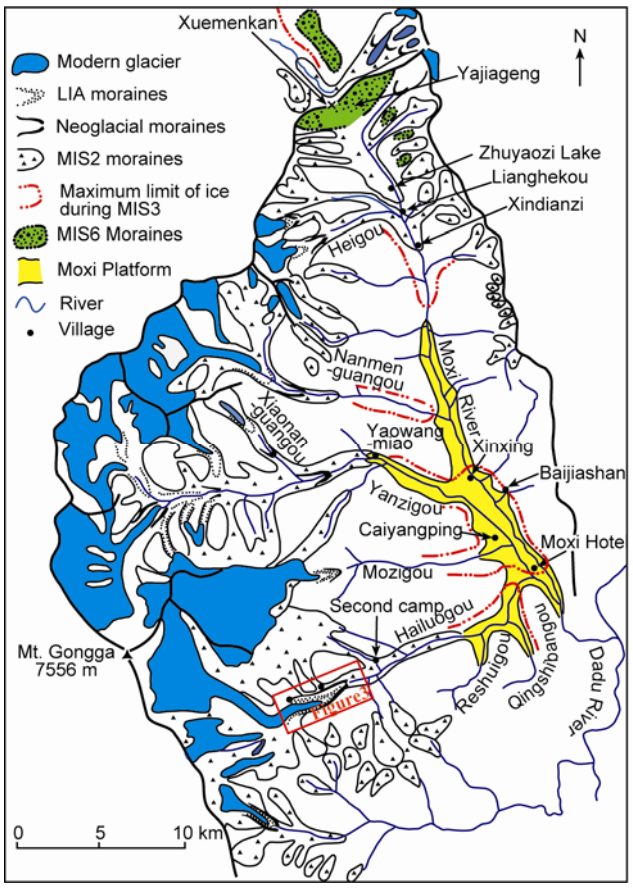

Figure 2 Geomorphological map of the eastern slope of Gongga Mountain (modified from ref. [22]).

The middle moraine ridge, which is the highest one, was assigned to the Dayanwo [18] or Guanjingtai glacial advance [21]. The outer and inner ridges were referred to as the HLG [18] and Qianguanjingtai glacial advance [21], respectively. Large lateral moraines, which rise 80–160 m above the glacier surface and extend to 3580 m a.s.l., are also present on both flanks of the YZG Glacier.

In the HLG valley, the third set of moraines is a morainic platform located at altitudes from 1850 to 3000 m a.s.l. on the northern side of the valley. This glacial advance was termed the HLG [16, 17] or Gongga Glaciation [27]. The well-exposed section near the Reshuigou valley is divided into three unconformable strata. The upper and lower strata are gray tills, and the middle stratum, approximately 4 m thick, is sandy silt associated with the fluvial-lacustrine facies. In the YZG valley, this moraine set is mainly preserved at Zhujiaping on the northwestern side of Yaowangmiao. Based on the remote sensing image, a U-shaped valley, approximately 4 km long, is identified on the northeast of the MZG Glacier's terminus (Figure 1). This suggests that a part of the MZG Glacier possibly flowed northeastward into the YZG valley during the HLG Glaciation. The moraines, which were deposited by the glaciers coming from near Xuemenkan during this glaciation, extend to 3100 m a.s.l. north of Lianghekou and blocked the Moxi River, resulting in the formation of the Zhuyaozi Lake. Meanwhile, the lateral moraines deposited by the Heigou Glacier also extend down valley to Xindianzi at an altitude of 2950 m a.s.l. [22].

The fourth set of moraines consists of the morainic platform, end moraines or hummocky moraines distributed on at the valley mouth and on the piedmont (Figure 2). In the HLG valley, this moraine set is mainly preserved between Banzhuyuan and the east side of Shanshuping. During that period, the Qingshibangou Glacier joined the HLG Glacier, and extended to near the HLG valley mouth, but could not flow into the Moxi River valley [22]. This moraine set is a

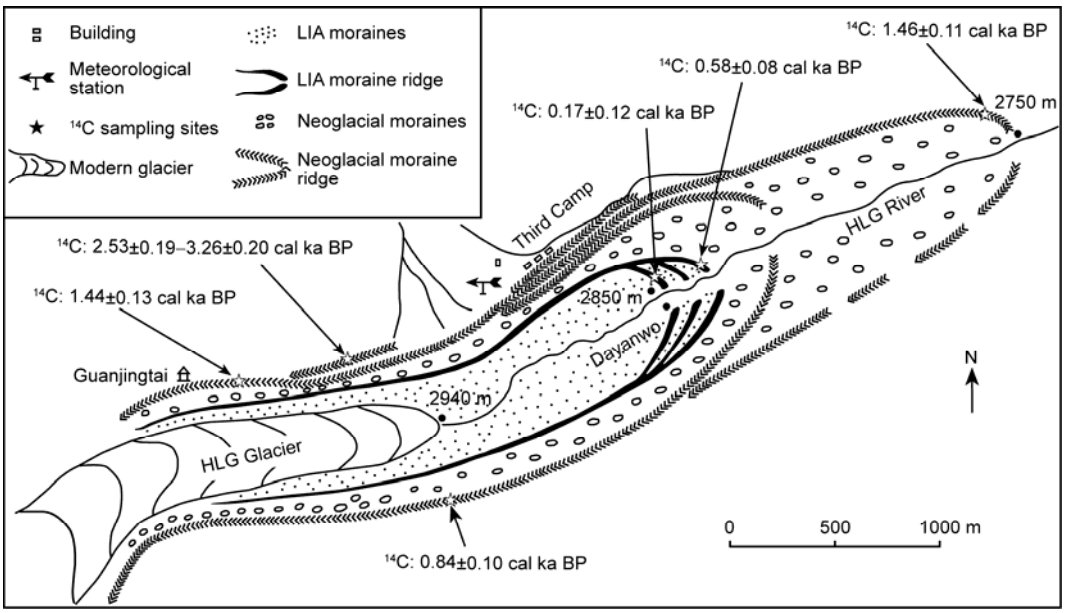

Figure 3 Little Ice Age (LIA) and Neoglacial moraines in the HLG valley (modified from ref. [21]).

morainic platform, which is preserved at Yuejinping on the north side of the NMGG valley mouth and is covered by reddish-brown soil. Boulders, some larger than 2 m in diameter, are scattered on its surface. The glacial advance was named the NMGG Glaciation by Wang et al. [19]. In addition, this moraine set is also preserved on both sides of the YZG valley below Yaowangmiao. Here, the till clasts are poorly sorted and semi-cemented. At the time these moraines were deposited, the YZG and MZG glaciers joined together in the Moxi River valley, and extended down valley to approximately 1550 m a.s.l. [22].

The fifth set of moraines, which is usually present at the valley source and the higher elevation, is not well-preserved due to erosion following deposition. There is a morainic platform on east side of the Yajiageng-Caopingzi, which has altitudes of 3700–3800 m a.s.l., a thickness of approximately 100 m, and rises approximately 30 m above the river bed. The till clasts are deeply weathered, and there is a brown weathering layer of 3–5 mm in thickness present on their surfaces. The gravels of 20 cm in diameter are easily crushed by a hammer. This glacial advance was referred to as the Yajiageng Glaciation [15, 19]. Based on the reconstructed extent of this moraine set, the paleoglaciers that prevailed during this glaciation were piedmont glaciers.

2.2 Glaciofluvial sediments

The Moxi Platform is located between Xinxing and the Moxi, with a length of approximately 10 km, widths of 1–2 km and a thickness of approximately 120 m (Figures 2 and 4). It consists of sand and gravel, and is formed by the glacial, glaciofluvial and debris flow deposits coming from the YZG, MZG and HLG valleys [21]. Multiple glaciofluvial terraces and fan-shaped landforms are well developed along the valleys of the eastern slope. On the basis of our field investigations and the analysis of previous literature, it is very clear that this platform and the terraces along both sides have a tight relationship with the meltwater and, glacial advance and retreat after the NMGG Glaciation.

The sub-angularity and poor sorting of alluvial deposits in this region are typically associated with small, steep mountain streams which flow through this till-covered region. Accumulation and incision of the Moxi River lead to the development of four terraces on the eastern side of the platform. They rise approximately 5–10 m (T_1), 35 m (T_2), 65 m (T_3) and 85m (T_4) above the contemporary river bed on the eastern side of Xinxing. On the basis of the sedimentary facies, the fourth terrace can be divided into 13 stratigraphic intervals including gravel, sandy and silt layers [21]. The gravels of the lowest and seventh layers reach up to 40 cm in diameter. Terrace sequences also developed in the YZG and the HLG valleys. Their heights rising above the contemporary river bed are 5–10, 30, 50 and 100 m near Yaowangmiao, and 5–10, 30, 90 and 140 m in the HLG valley mouth. The T_1 and T_2 between the First Camp and the Second Camp are preserved adjacent to the third set of moraines.

3 Methods

OSL and ESR dating samples were collected from the natural and man-made sections on the eastern slope of Gongga Mountain (Figure 1). In addition, the published ^{14}C ages from moraines and glaciofluvial deposits in this region were compiled and calibrated into calendar years by using the program CALIB Rev. 6.1.0 based on IntCal09 calibration dataset [28] (Table 2).

3.1 OSL dating

The OSL samples were prepared and tested in the chronology laboratory at the Key Laboratory of Western China's Environmental System (Ministry of Education), using the procedures described by Li et al. [29]. Isolation of quartz (90–125 mm) from the samples was performed under subdued red light in the laboratory. Luminescence measurements were undertaken using an automated TL/OSL reader (RisφDA-15), and equivalent doses (D_e) were estimated using the single-aliquot regenerative-dose (SAR) protocol [30] (Figure 5). For dose rate calculation, the U, Th and K contents of the samples were determined using neutron ac-

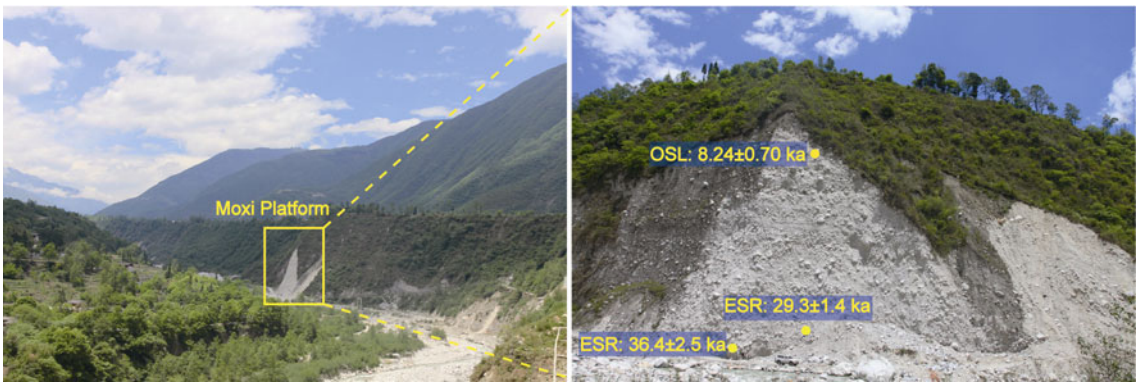

Figure 4 Moxi Platform and section on the opposite of Caiyangping.

Table 2 ^{14}C ages from moraines and glaciofluvial deposits on the eastern slope of Gongga Mountain

Sample's location	Dating materials	^{14}C age (a BP)	Calibrated ^{14}C age (cal ka BP-2σ range)	Source
The outermost ridge of the first moraine set in the HLG valley	Buried wood	540±70	0.58±0.08	[21]
The innermost ridge of the first moraine set in the HLG valley	Buried wood	150±60	0.17±0.12	[21]
The innermost ridge of the second moraine set in the HLG valley	Buried wood	940±50	0.84±0.10	[18]
The middle ridge of the second moraine set in the HLG valley	Buried wood	1550±70	1.44±0.13	[21]
The middle ridge of the second moraine set in the HLG valley	Buried wood	1580±60	1.46±0.11	[18]
The outmost ridge of the second moraine set in the HLG valley	Buried wood	2430±80–3080±80	2.53±0.19–3.26±0.20	[21]
Lateral moraines 2 km from the Xiaonanguangou (XNGG) Glacier	Buried wood	780±90	0.77±0.14	[21]
The middle layer of the third moraine set near the Reshuigou valley	Buried soil	24390±750	29.25±1.51	[19]
The upper layer of the third moraine set near the Reshuigou valley	Inorganic carbonate coating	17900±300	21.31±0.85	[18]
The bottom of T_4 on the eastern side of Xinxing	Buried soil	7240±90–7430±300	8.22±0.29–8.25±0.57	[17]
The bottom of T_2 near Baijiashan	Buried wood	2350±95	2.46±0.17	[17]
The upper layer of T_2 1 km upward from Yaowangmiao	Buried wood	1490±70	1.41±0.12	[17]
T_1 near the XNGG valley	Buried wood	732±30	0.69±0.04	[16]
The gravel layer of T_1 near Guanjingtai	Buried wood	930±30	0.85±0.07	[21]
The gravel layer of T2 near Guanjingtai	Buried soil	1200±70–2170±60	1.13±0.15–2.18±0.15	[21]
Ruoguo glacial advance on the southeastern Tibet	Buried wood	1540±85–1920±110	1.45±0.16–1.87±0.27	[48]

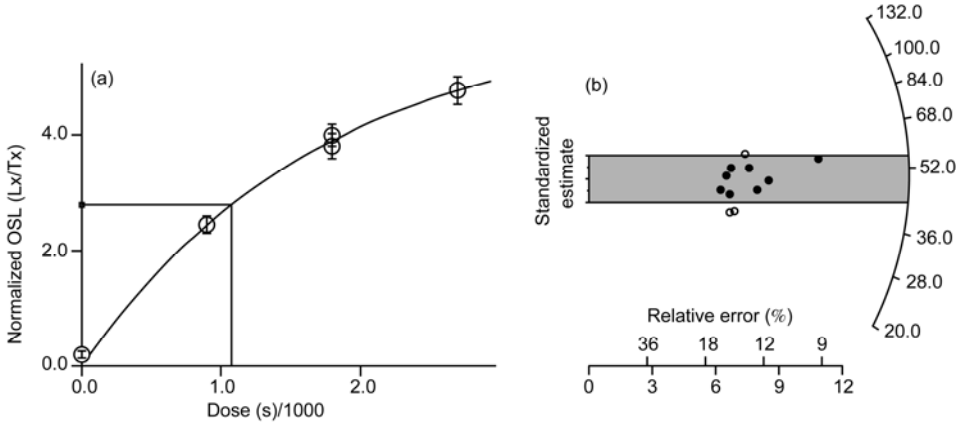

Figure 5 The growth curve (a) and radial plot (b) for OSL of sample GGS-04.

tivation analysis (NAA) at the China Institute of Atomic Energy. The cosmic ray contribution to the dose rate was calculated using the function suggested by Prescott and Hutton [31]. The OSL dating results and correlated parameters are listed in Table 3.

The assumption of OSL dating techniques is that the dating signals in mineral grains were bleached during the last process of sediment reworking, transportation and deposition. For OSL dating, the glacial sediments were considered to be partially bleached deposits [33–35]. Ice flow of mountain glaciers is characterized by multiple longitudinal compressive and extending flows. Debris carried by the glaciers has many opportunities to experience exposure to daylight along the slip planes; increasing the probability of complete resetting the luminescence signal [32]. Because of this, glaciofluvial deposits are more suitable for the OSL dating than the glacial tills [33]. Therefore, appropriate measurement techniques and sampling strategies represent the first important, and often neglected, step in overcoming sufficient bleaching and obtaining reliable luminescence ages [33–35]. For 3 of the 4 samples, which were collected from a sandy lens, their ages are consistent with their stratigraphic sequence, and published ^{14}C and TCN ^{10}Be ages. The GGS-02 collected from tills is inconsistent with the geological setting and significantly older than the ages of other samples from the same moraine set. It is likely that it is an outlier that has erroneous age due to insufficient bleaching.

3.2 ESR dating

The ESR samples, generally collected from sandy lenses in moraines, were kept in opaque plastic bags to ensure that they were not exposed to sunlight. Grinding, collision and heating were also avoided during transportation. The samples were prepared in the chronology laboratory at the Key Laboratory of Western China's Environmental System (Ministry of Education). Previous studies have shown that the signal intensity of the Ge centers in quartz grains exposed under natural room light does not decrease [36, 37],

Table 3 OSL and ESR dating results and the correlated parameters and sampling sites

Sample No.	Lab No.	Samples' locations and description					U (ppm)	Th (ppm)	K (%)	Cosmic (Gy/ka)	Water (%)	D_e (Gy)	Age (ka)
		Longitude (E)	Latitude (N)	Altitude (m a.s.l.)	Sample's description	Depth (m)							
GGS-01[a)]	Lzu1025	101°55.257′	29°40.808′	3702	Till of the lateral moraines on the southeast of the YZG Glacier	2.5	4.15±0.14	16.5±0.43	2.70±0.08	0.30	4.69	10.87±2.48	2.2±0.5
GGS-02[a)]	Lzu1026	102°55.502′	29°40.967′	3535	Till of the end moraines 2 km from YZG Glacier's terminus	3.1	7.96±0.20	22.7±0.57	3.04±0.09	0.27	2.06	215.77±10.67	32.4±2.5
GGS-03[a)]	Lzu1027	102°07.930′	29°38.527′	1459	Glaciofluvial lens from the bottom of the Moxi Platform near the power plant	15.0	4.76±0.14	18.3±0.48	3.52±0.10	0.06	3.66	333.51±14.37	58.0±4.3
GGS-04[a)]	Lzu1028	102°06.695′	29°39.333′	1549	Glaciofluvial deposits from the upper layer of the Moxi Platform	7.0	4.67±0.15	21.3±0.53	3.44±0.10	0.11	4.70	49.06±2.88	8.2±0.7
YJG-01	9368	102°00.811′	29°53.783′	3919	Sandy lens from the moraines of the Yajiageng Glaciation	2.7	1.38±0.12	6.30±0.18	1.71±0.07	0.24	7.46	259.58±11.96	94.5±13.3
YJG-02	9369	102°01.064′	29°53.280′	3778	Sandy lens from the moraines of the Yajiageng Glaciation	3.2	0.86±0.11	4.00±0.14	1.18±0.06	0.21	6.65	272.61±5.51	142.8±18.7
YJG-03	9370	102°01.070′	29°53.276′	3780	Sandy lens from the moraines of the Yajiageng Glaciation	4.5	0.65±0.12	2.86±0.12	1.14±0.06	0.18	7.33	264.49±10.80	156.9±25.0
YJG-04	9371	102°01.085′	29°53.161′	3718	Sandy lens from the moraines of the Yajiageng Glaciation	4.0	0.95±0.13	3.62±0.14	1.17±0.06	0.19	8.09	253.29±3.83	137.7±15.7
YJG-05	9372	102°01.256′	29°52.766′	3623	Sandy lens from the moraines of the Yajiageng Glaciation	3.0	0.82±0.11	3.94±0.14	1.16±0.06	0.22	9.20	218.57±5.53	119.2±15.9
YJG-06	9373	102°01.257′	29°52.765′	3622	Till of Yajiageng Glaciation	5.6	1.27±0.13	5.06±0.16	1.07±0.05	0.14	9.77	358.73±16.52	194.2±32.8
YJG-07	9374	102°01.486′	29°52.522′	3611	Sandy lens from the moraines of the Yajiageng Glaciation	3.0	1.0±0.12	5.41±0.18	1.33±0.06	0.21	7.89	311.04±11.08	142.2±21.5
NMG-01	9375	102°04.122′	29°43.854′	2071	Till on the north of the Nanmeguangou valley mouth	4.2	2.80±0.28	27.40±0.77	3.45±0.10	0.14	6.45	339.72±20.67	53.6±4.7
NMG-02	9376	102°03.984′	29°43.880′	2090	Sandy lens from the moraines of the north of the NMGG valley mouth	5.0	3.56±0.28	28.67±0.75	3.46±0.10	0.12	3.60	244.44±12.54	35.9±2.7
YZG-02	9379	102°00.371′	29°41.981′	2574	Till at Zhujiaping	3.7	4.3±0.30	42.14±1.01	4.15±0.11	0.15	12.72	94.48±1.48	11.9±0.6
YZG-03	9380	102°03.547′	29°41.458′	2109	Sandy lens from the moraines of the north of the YZG valley mouth	3.2	7.07±0.35	38.16±0.92	3.86±0.11	0.16	6.69	417.56±36.46	48.5±4.9
YZG-04	9381	102°03.548′	29°41.459′	2109	Till from the north of the YZG mouth	1.5	5.14±0.28	25.21±0.71	3.46±0.10	0.23	6.78	396.35±31.58	58.0±6.3
MX-01	9382	102°06.944′	29°39.337′	1571	Sandy lens from the lower layer of the Moxi Platform on the opposite of Caiyangping	30.5	4.04±0.27	51.33±1.18	3.34±0.10	0.00	1.86	251.17±9.21	29.3±1.4
MX-03	9384	102°06.944′	29°39.337′	1573	Sandy lens from the lower layer of the Moxi Platform on the opposite of Caiyangping	32.0	2.70±0.26	24.16±0.68	3.72±0.11	0.00	4.33	231.16±13.70	36.4±2.5

a) OSL dating.

therefore all samples were treated under natural room light conditions. The sample preparations and measurements follow the literature [38, 39].

The prepared samples were irradiated by ^{60}Co with different doses with a dose rate of 28.51 Gy min^{-1}. The irradiated samples were tested in the chronology laboratory at the Institute of Geology, China Earthquake Administration, Beijing. The Ge centers in the quartz grains were chosen as dating signals and were measured with an EMX1/6ESR spectrometer manufactured by Bruker (Germany). The measurement conditions and parameters were as follows: room temperature, X-band, microwave power=2.021 mW, central magnetic field=3525 G, sweep width=50 G, frequency=9.852 GHz, modulation frequency=100 kHz, modulation amplitude=1 G (1 G=10–4 T), time constant= 40.96 ms, and sweep time =10.486 s. It is obvious that the signal intensity of the Ge centers increased with an increased dose of artificial irradiation. A least-squares analysis was used to fit the data points on the basis of different artificial irradiation doses and corresponding signal intensities. Linear fits were chosen in this study. The line was then extrapolated to zero in order to obtain the D_e (Figure 6). The concentrations of U and Th and the content of K_2O were determined by neutron activation analysis (NAA) at the China Institute of Atomic Energy. The annual dose rate was estimated from these radioactive elements, the water content, and the estimated cosmic ray contribution and calculated following the formulas suggested by Prescott and Hutton [31]. The ESR dating results and correlated parameters are listed in Table 3.

Previous studies have shown that Ge centers are sensitive to sunlight and grinding, and these two mechanisms are capable of effectively removing them [40–42]. According to the theory of the structure and the movement of mountain glaciers [43], exposure of glacier carried debris to sunlight is possible. The debris is also subject to grinding during this movement, and the high silt content in glacial deposits could support this [44, 45]. Second, the absorption band of Ge centers is 4.43 eV [46], corresponding to a wavelength of 280 nm. This wavelength produces higher levels of energy in the Ge absorption band at higher elevations. The dating samples were collected from a region at high elevation. Therefore, the ESR signals of the Ge centers in glacial quartz grains could be removed. Previous studies have shown that ESR dating results are reliable and credible, and that this technique can be applied to Quaternary glaciation research [4, 5, 7, 38, 39, 47]. As for the ages of 14 samples, with exception of YJG-01, their ages are tightly clustered, and consistent with their stratigraphic sequence and the OSL ages of corresponding glaciofluvial deposits. YJG-01 is significantly younger than the cluster ages from the same moraine set. This is possibly because it is close to the tributary valleys on the east of Yajiageng and hence may be reshaped by the younger glaciations from these tributary valleys.

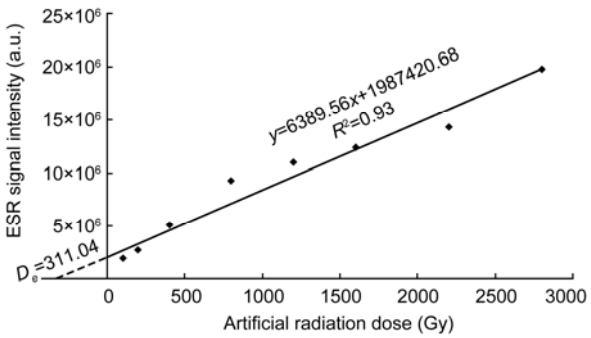

Figure 6 Best-fit line between artificial radiation doses and ESR signal intensity (YJG-07).

4 Results and discussion

4.1 Chronology of glaciations

Buried wood within the innermost and outermost moraine ridges of the first moraine set in the HLG valley have ^{14}C ages of 0.17±0.12 cal ka BP and 0.58±0.08 cal ka BP, respectively [21]. Therefore, it is reasonable to conclude that the first set of moraines was deposited during the Little Ice Age (LIA).

Within the second moraine set, the ^{14}C age is 0.84±0.10 cal ka BP for the outmost moraine ridge of the second set [18]; 1.44±0.13–1.46±0.11 cal ka BP for the middle ridge [18, 21], which is equivalent in age to the Ruoguo glacial advance (1.45±0.16–1.87±0.27 cal ka BP) in southeastern Tibet [48]; and 2.53±0.19–3.26±0.20 cal ka BP for the outmost ridge, which is equivalent in age to the Xuedang glacial advance in southeastern Tibet [21]. During that period, the HLG Glacier was 3 km longer than the modern glacier. These ^{14}C dates are consistent with the TCN ^{10}Be surface exposure ages of the first and second moraine sets in the HLG valley [11]. The ^{14}C age for buried wood within the moraines (3200 m a.s.l.) in the XNGG valley is 0.77±0.14 cal ka BP [21]. The OSL sample (GGS-01) from the huge lateral moraines in the YZG valley date to 2.2±0.5 ka. These above-mentioned ages suggest that the second set of moraines was formed during the Neoglaciation.

The ^{14}C age is 29.25±1.51 cal ka BP for the middle silt layer [19], and 21.31±0.85 cal ka BP for the calcareous sinter covering on the upper moraines near the Reshuigou valley [18]. The ESR sample collected from the moraines near Zhujiaping date to 11.9±0.6 ka. The TCN ^{10}Be surface exposure ages (7.94±0.68–9.15±0.50 ka) for the third moraine set in the HLG valley [11], are significantly younger than these ages. However, these exposure ages likely represent the timing of glacier retreat. In addition, they are not corrected for boulder surface erosion, which can decrease TCN concentration. Previous studies suggest that the mean erosion rate of the boulder surface is up to 27.1±10.2 mm ka^{-1} in southeastern Tibet since the Last Interglacial [49], where

the precipitation is similar to that of Gongga Mountain. Therefore, we can conclude that the surface of the boulders experienced intensive erosion in Gongga Mountain. This would result in significantly underestimating of the true exposure age. In view of these ages, the authors consider that the third set of moraines was deposited during the global Last Glacial Maximum (LGM_G) in MIS2.

Based on the stratigraphic sequence of the fourth moraine set, in addition to a comparison with the chronology of glacial successions in adjacent regions, previous studies postulated that the fourth moraine set was possibly deposited during the penultimate glacial cycle corresponding to MIS6 [22, 23]. However, two ESR samples collected from the Yuejingping morainic platform date to 35.9±2.7 and 53.6±4.7 ka and another two ESR samples from the moraines on the northern side of the YZG valley mouth date to 48.5±4.9 and 58.0±6.3 ka. These ages indicate that the fourth moraine set was deposited during the middle part of the last glacial cycle corresponding to the mid-MIS3. The location of this moraine set and the associated ages suggest that the largest local last glacial maximum (LGM_L) in this region should have occurred during mid-MIS3 rather than the LGM_G in MIS2.

As more extensive and reliable numerical dates became available, Gillespie and Molnar [50] reviewed published evidence from over 50 glaciated mountain areas around the world. They found that the glaciation in the Himalaya and Tibetan Plateau was asynchronous with the maximum extent of the Northern Hemisphere ice sheets. In particular, it appears that in many regions, such as the Hunza valley, Khumbu Himal and NE Tibet, glaciers reached their maximum extent during the insolation maximum of MIS3. Subsequently, the studies of Phillips et al. [51] and Owen et al. [6] partly confirmed this view in the southern margin of the Tibetan Plateau which is climatically dominated by the south Asian monsoon. Recent geomorphological and chronological evidence shows that glacial advances also occurred during MIS3 in other regions climatically dominated by monsoon circulation, such as the Shaluli Mountains [4], Queer Shan [52], Anyemaqen Mountains [10], Nianbaoyeze Mountains [10] and Shesan Mountain [53]. The $\delta^{18}O$ records in Guliya ice core show that an intense temperature fluctuation occurred during MIS3 [54] (Figure 7(c)). The temperatures in early and late parts of MIS3 were 3 and 4°C higher than the present, respectively. However, the mid-MIS3 was an obvious cold period; the temperature dropped 5°C lower than the present [55]. The paleotemperatures inferred from the oxygen isotope record of the RM core from the Zoigê Basin on the eastern margin of the Tibetan Plateau also indicate the mid-MIS3 was a cold period [56] (Figure 7(d)), in which two significantly cold events occurred at approximately 45 ka and 48 ka cold (corresponding to the Heinrich 5 event) [57]. Recent studies suggest that the higher insolation during MIS3 can result in an intensified south Asian summer monsoon, and thus increased the supply of monsoon precipitation as snow at high altitudes [6, 50, 55] (Figure 7(f)). Geomorphologic and sedimentological evidence also show that high lake levels

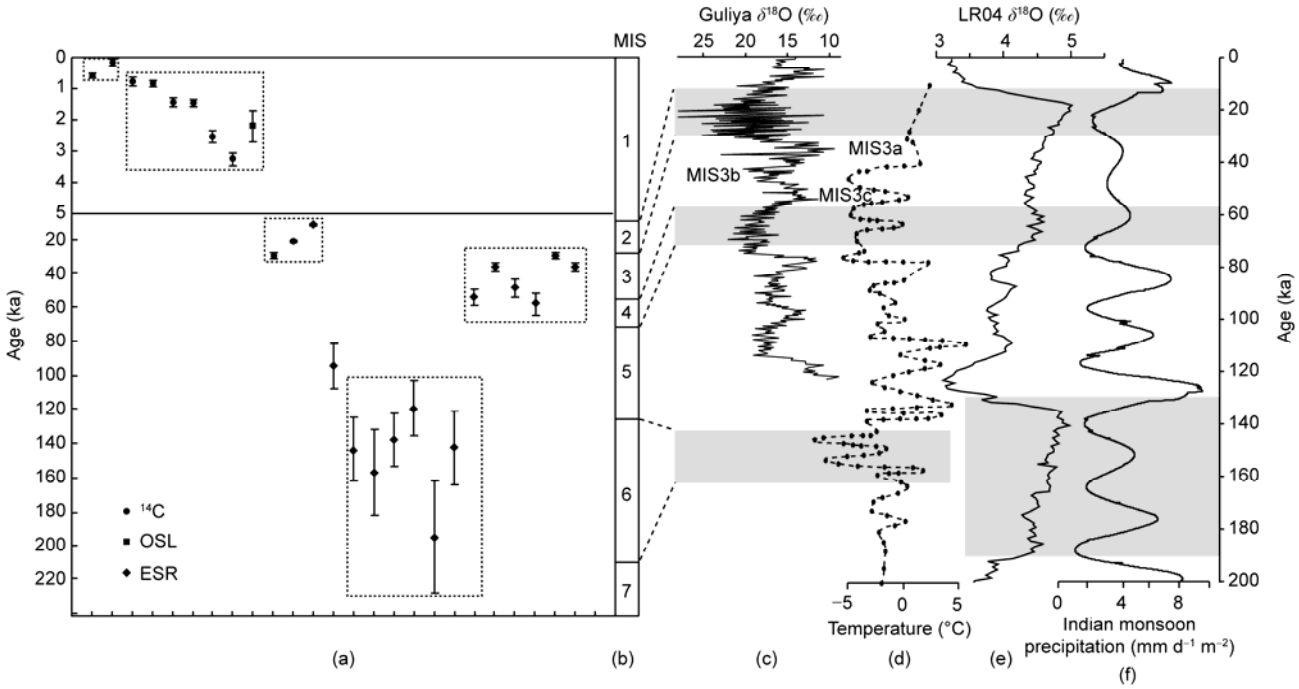

Figure 7 A comparison of Quaternary glacial chronology on the eastern slope of Gongga Mountain with different records. (a) Dating results and their errors; (b) marine oxygen-isotope stages (MIS); (c) the $\delta^{18}O$ record in the Guliya ice core [54]; (d) the RM core from the Zoigê Basin [56]; (e) the LR04 benthic $\delta^{18}O$ records [61]; (f) modeled Indian monsoon June-July-August precipitation by CLIMBER II [62].

and large fresh-water lakes occurred in the Tibetan Plateau during late and mid-MIS3 [58, 59]. It is likely that the cold-humid climate of mid-MIS3 produced positive glacier mass balances, therefore allowing glaciers to advance. During the LGM_G, precipitation (approximately 250 mm) was only approximately 40% of present values on the southeastern Tibetan Plateau [60], which would have restricted ice accumulation despite the low temperatures during this period (Figure 7(c) and (e)). This is the reason that glaciation was more extensive during mid-MIS3 than during the LGM_G.

The ESR ages for 7 samples from the moraines near Yajiageng, with the exception of YJG-01, range from 119.2±15.9 to 194.2±32.8 ka (YJG-02–07) (Table 2). The dating results suggest that the fifth moraine set (Yajiageng Glaciation) was deposited during the penultimate glaciation, corresponding to MIS6, rather than during the antepenultimate glaciation (the early part of mid-Pleistocene) as previously thought. The LR04 stacked benthic $\delta^{18}O$ curve shows that MIS6 was a significant cold period [61] (Figure 7(e)). The paleo-temperatures reconstructed from the RM core also indicate an intense temperature decrease (approximately 4.3°C lower than present) during this time period [57] (Figure 7(d)).

It is possible that Gongga Mountain, the highest mountain on the eastern part of the Tibetan Plateau, experienced a glaciation prior to MIS6, but evidence supporting this idea has not been found thus far. The temperate glaciers of Gongga Mountain have the characteristics of rich accumulation and ablation, enhanced subglacial erosion and, high transportation and deposition rates, and as a result are more sensitive to the changing climate. During climate warming, a combination of abundant precipitation and the significant increase in glacier meltwater would result in frequent floods and debris flows. Furthermore, most of this region is characterized by steep slopes greater than 30°. The intense denudation, mainly by fluvial and mass movement processes, would result in rapid erosion and re-sedimentation of glacial and associated landforms in this region, contributing more to the lack of preservation here than in regions of greater aridity. However, it is still worth further examination to see whether moraines older than MIS6 are preserved in this region.

4.2 Mechanism of formation of the Moxi Platform

The Kangding-Moxi regional fault crosses Xuemengkan and Moxi, and intersects with the east-west faults of the HLG, MZG, and YZG valleys. The Moxi River valley was formed as result of the erosion and incision along the Kangding-Moxi fault, by glaciers, precipitation and mass wasting [16, 63]. The part of the Moxi Platform below the Moxi Hotel consists of subhorizontally bedded glaciofluvial deposits. Many granite and metamorphic erratic boulders (10–20 m in diameter), which are bullet-shaped and edge-rounded with occasional striations, are scattered on the surface of the Moxi Platform around Xinxing. However, contention still exists over the mechanism and the timing of formation of the Moxi Platform because previous researchers have not been able to definitively determine them. Heim, for example, considered that the Moxi Platform was formed by the deposition of glaciofluvial sediments during the last glacial cycle [12]. Li [64] proposed three possible mechanisms of formation: bottom moraines deposited by glaciers, diluvium deposited by floods during climate warming, and alluvium from the intense erosion and incision during uplift of the mountain. In addition, Cui suggested that the bottom of the platform contained non-glaciofluvial deposits, most likely older tills [14]. Based on fieldwork (1979–1980) along with the sedimentary evidence of the platform and the terraces on both sides, the Institute of Mountain Hazards and Environment Chinese Academy of Sciences concluded that the platform was an alluvial terrace with occasional debris flow deposits formed during the early Holocene [16]. Recently, Zheng [22] suggested that the main part of the platform consists of tills associated with the NMGG Glaciation occasionally mixed with lacustrine sediments and lenses of glaciofluvial sandy gravel, while most surface boulders on the platform were derived from supraglacial melt-out till, and the others were transported by glacial debris flows (re-sedimentation of glacial deposits).

There are some erratic boulders scattered on the slope east of the Moxi Upper Street. The sedimentary facies of several sections show that the platform near the Moxi Lower Street consists of ablation till occasionally mixed with glacial debris flow deposits [22]. The platform surface between Xinxing and the Moxi Lower Street does not exhibit a continuous declining slope down valley associated with the shape of a terrace surface, but instead exhibits a stepwise declining slope similar to the shape of a series of morainic platforms formed by multiple terminations when glacier retreated from its maximum extent. These evidence above-mentioned suggest that the paleoglaciers of the YZG and MZG valleys had extended to the Moxi Lower Street north of the Moxi Hotel during the NMGG Glaciation. In addition, lacustrine sediments are widely present between Xinxing and the NMGG valley [22]. Therefore, we concluded that the paleoglaciers likely had blocked the Moxi River valley and formed a moraine-dammed lake in this region.

Previous studies provide a series of ^{14}C ages for the wood buried within the terraces next to the platform as follows (Table 2): 8.22±0.29–8.25±0.57 cal ka BP from the brown silt at the bottom of T_4 on the eastern side of Xinxing [17], 2.46±0.17 cal ka BP from the bottom of T_2 near Baijiashan [17], 1.41±0.12 cal ka BP from the upper and middle layers of T_2 1 km upward from Yaowangmiao [17], 0.69±0.04 cal ka BP from the T_1 near the mouth of the XNGG valley [16], 0.85±0.07 cal ka BP from the gravel layer of T_1 and 1.13±0.15–2.18±0.15 cal ka BP from the gravel layer of T_2 near Guanjingtai in the HLG valley [21]. These dates indi-

cate that the terraces are probably correlative with meltwater after the last glacial cycle. The OSL age for sample GGS-04 from the upper layer of the Moxi platform across from Caiyangping is 8.2±0.7 ka, and the TCN ^{10}Be ages of the platform surface is 3.27±0.43–6.27±0.47 ka [11]. In addition, two ESR ages for the middle and lower layers are 29.3±1.4 and 36.4±2.5 ka, and the OSL age for the bottom of the platform near the power plant is 57.99±4.34 ka. Therefore, on the basis of geomorphological, sedimentological, and compositional characteristics, landforms of the Moxi Platform and terraces can be grouped by facies and geochronology. In combination with the dating results, this analysis indicates that the basal part of the Moxi Platform between Xinxin and the Moxi Hotel is correlative with the till of the Nanguanmen Glaciation (mid-MIS3). This basal unit has occasional lenses of glaciofluvial sandy gravel and lacustrine sediments. The remainder of the Moxi Platform and the terraces beside the platform are glaciofluvial deposits mixed occasionally with debris flow deposits and with a chronological range from MIS3 to Holocene.

5 Conclusions

Five glacial advances in this region have been identified, which are equivalent in age to the Little Ice Age (LIA), Neoglaciation, marine oxygen isotope stage (MIS) 2, mid-MIS3, and MIS6. The largest local last glacial maximum (LGM_L) occurred on Gongga Mountain during mid-MIS3, characterized by a cold-humid climate, rather than the global Last Glacial Maximum (LGM_G) of MIS2. The Gongga, Nanmenguangou (NMGG) and Yajiageng Glaciations occurred during the late part of the last glacial cycle, the middle of the last glacial cycle and the penultimate glacial cycle, respectively. The basal part of the Moxi Platform between Xinxin and the Moxi Hotel is correlative with the till of the Nanguanmen Glaciation (mid-MIS3). This basal unit has occasional lenses of glaciofluvial sandy gravel and lacustrine sediments. The remainder of the Moxi Platform and the terraces beside the platform are glaciofluvial deposits occasionally mixed with debris flow deposits ranging in age MIS3 to Holocene.

We thank Li Jianping with Institute of Geology, China Earthquake Administration, Ni Bangfa with China Institute of Atomic Energy and Fan Yuxin with Lanzhou University for helping date the samples. We are grateful to three anonymous reviewers for their constructive comments. This work was supported by National Natural Science Foundation of China (Grant No. 41171063), Fundamental Research Funds for the Central Universities (Grant No. LZUJBKY-2010-114), Foundation of State Key Laboratory of Cryospheric Sciences, Cold and Arid Regions Environment and Engineering Research Institute, Chinese Academy Sciences (Grant No. SKLCS 2011-03) and the Program of Ministry of Science and Technology of China (Grant No. 2006FY110200).

1 Cui Z J, Zhang W. Discussion about the glacier extent and advance/retreat asynchrony during the Last Glaciaiton (in Chinese). J Glaciol Geocryol, 2003, 25: 510–516
2 Zhou S Z, Xu L B, Wang J, et al. A preliminary study on timing of the oldest Pleistocene glaciation in Qinghai-Tibetan Plateau. Quat Int, 2006, 154/155: 44–51
3 Zhou S Z, Xu L B, Colgan P M, et al. Cosmogenic ^{10}Be dating of Guxiang and Baiyu Glaciations. Chin Sci Bull, 2007, 52: 1387–1393
4 Xu L B, Zhou S Z. Quaternary glaciations recorded by glacial and fluvial landforms in the Shaluli Mountains, Southeastern Tibetan Plateau. Geomorphology, 2009, 103: 268–275
5 Yi C L, Li X Z, Qu J J. Quaternary glaciation of Puruogangri—the largest modern ice field in Tibet. Quat Int, 2002, 97/98: 111–121
6 Owen L A, Finkel R C, Caffee M W. A note on the extent of glaciation throughout the Himalaya during the global Last Glacial Maximum. Quat Sci Rev, 2002, 21: 147–157
7 Wang J, Zhou S Z, Zhao J D, et al. Quaternary glacial geomorphology and glaciations of Kongur Mountain, eastern Pamir, China. Sci China Earth Sci, 2011, 54: 591–602
8 Zhang W, Niu Y B, Ling Y, et al. Late Pleistocene glaciation of the Changbai Mountains in northeastern China. Chin Sci Bull, 2008, 53: 2672–2684
9 Seong Y B, Owen L A, Yi C L, et al. Quaternary glaciation of Muztag Ata and Kongur Shan: Evidence for glacier response to rapid climate changes throughout the Late Glacial and Holocene in westernmost Tibet. Geol Soc Am Bull, 2009, 121: 348–365
10 Owen L A, Finkel R C, Ma H Z, et al. Timing and style of late Quaternary glaciation in northeastern Tibet. Geol Soc Am Bull, 2003, 115: 1356–1364
11 Owen L A, Finkel R C, Barnard P L, et al. Climatic and topographic controls on the style and timing of Late Quaternary glaciation throughout Tibet and the Himalaya defined by ^{10}Be cosmogenic radionuclide surface exposure dating. Quat Sci Rev, 2005, 24: 1391–1411
12 Heim A. The glaciation and solifluction on Minya Gongkar. Geogr J, 1936, 87: 444–454
13 Anderson J G. Topographical and archaeological studies in the Far East. The Museum of Far Eastern Autiquities (Ocstasiatiska Samligarna). Stockholm Bull, 1939, 11: 7–22
14 Cui Z J. Preliminary observation of present glaciers in the Mt. Gongga (in Chinese). Acta Geol Sin, 1958, 24: 318–338
15 Fan W J. The geological tectonic foundation of Minya Gongkar and its characteristic glacial landforms (in Chinese). J Chengdu Univ Sci Technol, 1982, (3): 19–28
16 Liu S Z, Liu X M, Zhao Y T, et al. Geomorphology and its development in Gongga Mountain Region (in Chinese). In: Chengdu Institute of Geography, CAS, ed. Region Geographic Expedition in the Gongga Mountain. Chongqing: Chongqing Branch of Scientific and Technology Document Press, 1983. 21–34
17 Li Z W, Chen J L, Hu F D, et al. Geological structure of Gongga Mountain (in Chinese). In: Chengdu Institute of Geography, CAS, ed. Region Geographic Expedition in the Gongga Mountain. Chongqing: Chongqing Branch of Scientific and Technology Document Press, 1983. 4–20
18 Li J J, Song M K, Qing D H, et al. Investigation of glaciers on the Gongga Shan (in Chinese). In: Comprehensive Scientific Expedition Team of CAS in Qinghai-Tibetan Plateau, ed. Special Issue of Hengduan Mountains Expedition (I). Kunming: Yunnan People's Press, 1983. 140–153
19 Wang M L, Hu F D, Li Z W. Discuss of Quaternary glaciation on the Gongga Mountain (in Chinese). In: Gao S Z, Zheng Y C, eds. Research Papers in Hengduan Mountains. Chengdu: Sichuan Science and Technology Press, 1989. 50–58
20 Su Z, Liu S Y, Wang L L, et al. Recent fluctuations of glaciers in the Gongga Mountains. Ann Glaciol, 1992, 16: 163–167
21 Zheng B X, Ma Q H. The glacier variation, climatic change and the river valley development in the Holocene on the Gongga Mountain (in Chinese). Acta Geol Sin, 1994, 46: 500–508
22 Zheng B X. Study on the Quaternary glaciation and the formation of the Moxi Platform in the east slopes of the Mount Gongga (in Chi-

nese). J Glaciol Geocryol, 2001, 23: 283–291
23 Su Z, Shi Y F, Zheng B X. Quaternary glacial remains on the Gongga Mountain and the division of glacial period (in Chinese). Adv Earth Sci, 2002, 17: 639–647
24 Liu S Z. Geomorphological types and mapping on the Gongga Mountain (in Chinese). In: Comprehensive Scientific Expedition Team of CAS in Qinghai-Tibetan Plateau, ed. Special Issue of Hengduan Mountains Expedition (I). Kunming: Yunnan People's Press, 1983. 114–123
25 Pu J C. Glacier Inventory of China VIII, the Yangtze River Drainage Basin (in Chinese). Lanzhou: Gansu Culture Press, 1994. 117–129
26 Su Z, Liang D L, Hong M. Developing conditions, amounts and distributions of glaciers in Gongga Mountain (in Chinese). J Glaciol Geocryol, 15: 551–557
27 Zheng B X, Rutter N. On the problem of Quaternary glaciations, and the extent and patterns of Pleistonce ice cover in the Qinghai-Xizang (Tibet) Plateau. Quat Int, 1998, 45/46: 109–122
28 Reimer P J, Baillie M G L, Bard E, et al. IntCal04 terrestrial radiocarbon age calibration, 0–26 cal kyr BP. Radiocarbon, 2004, 46: 1029–1058
29 Li G Q, Zhao H, Fan Y X, et al. Improved method for quartz purification in OSL dating (in Chinese). Adv Earth Sci, 2008, 23: 284–289
30 Murray A S, Wintle A G. Luminescence dating of quartz using an improved single-aliquot regenerative-dose protocol. Radiat Meas, 2000, 32: 57–73
31 Prescott J R, Hutton J T. Cosmic ray contributions to dose rates for luminescence and ESR dating: Large depths and long-term time variations. Radiat Meas, 1994, 23: 497–500
32 Ou X J, Xu L B, Lai Z P, et al. Potential of quartz OSL dating on moraine deposits from eastern Tibetan Plateau using SAR protocol. Quat Geochronol, 2010, 5: 257–262
33 Fuchs M, Owen L A. Luminescence dating of glacial and associated sediments: review, recommendations and future directions. Boreas, 2008, 37: 636–659
34 Thrasher I M, Mauz B, Chiverrell R C, et al. Luminescence dating of glaciofluvial deposits: A review. Earth-Sci Rev, 2009, 97: 133–146
35 Duller G A T. Single grain optical dating of glacigenic deposits. Quat Geochronol, 2006, 1: 296–304
36 Walther R, Zilles D. ESR studies on bleached sedimentary quartz. Quat Geochronol-Quat Sci Rev, 1994, 13: 611–614
37 Rink W J. Electron Spin Resonance (ESR) dating and ESR applications in Quaternary science and archaeometry. Radiat Meas, 1997, 27: 975–1025
38 Zhao J D, Song Y G, King J W, et al. Glacial geomorphology and glacial history of the Muzart River valley, Tianshan range, China. Quat Sci Rev, 2010, 29: 1453–1463
39 Zhao J D, Liu S Y, He Y Q, et al. Quaternary glacial chronology of the Ateaoyinake River Valley, Tianshan Mountains, China. Geomorphology, 2009, 103: 276–284
40 Tanaka T, Sawada S, Ito T. ESR dating of late Pleistocene near-shore and terrace sands. In: Ikeya M, Miki T, eds. ESR Dating and Dosimetry. Tokyo: Ionics, 1986. 275–280
41 Buhay W M, Schwarcz H P, Grün R. ESR dating of fault gouge: The effect of grain size. Quat Sci Rev, 1988, 7: 515–522
42 Ye Y G, Diao S B, He J, et al. ESR dating studies of paleo-debris-flows deposition Dongchuan, Yunnan Province, China. Quat Sci Rev, 1998, 17: 1073–1076
43 Li J J. The formation mechanism and identification of mountain glacial geomorphology (in Chinese). In: Shi Y F, Cui Z J, Li J J, eds. Quaternary Glacier and Environment in East China. Beijing: Science Press, 1989. 13–26
44 Mahaney W C, Vortisch W, Julig P J. Relative differences between glacially crushed quartz transported by mountain and continental ice: Some examples from North America and East Africa. Am J Sci, 1988, 288: 810–826
45 Yi C L. Subglacial comminution: Evidence from microfabric studies and grain size analysis. J Glaciol, 1997, 43: 174–179
46 Jin S Z, Deng Z, Huang P H. Study on optical effects of quartz E' Center in loess. Chin Sci Bull, 1991, 36: 1865–1870
47 Zhao J D, Zhou S Z, He Y Q, et al. ESR dating of glacial tills and glaciations in the Urumqi River headwaters, Tianshan Mountains, China. Quat Int, 2006, 144: 61–67
48 Li J J, Zheng B X, Yang X J, et al. Glaciers in Tibet (in Chinese). Beijing: Science Press, 1986. 138–140
49 Xu L B, Zhou S Z. Quantifying erosion rates in the southeastern Tibetan Plateau since the last interglacial using *in-situ* cosmogenic radionuclide ^{10}Be (in Chinese). Acta Geol Sin, 2009, 83: 487–495
50 Gillespie A, Molnar P. Asynchronous maximum advances of mountain and continental glaciers. Rev Geophys, 1995, 33: 311–364
51 Phillips W M, Sloan V F, Shroder J F, et al. Asynchronous glaciation at Nanga Parbat northwestern Himalaya Mountains, Pakistau. Geology, 2000, 28: 431–434
52 Xu L B, Ou X J, Lai Z P, et al. Timing and style of Late Pleistocene glaciation in the Queer Shan, northern Hengduan Mountains in the eastern Tibetan Plateau. J Quat Sci, 2010, 25: 957–966
53 Cui Z J, Yang C F, Liu G N, et al. The Quaternary glaciation of Shesan Mountain in Taiwan and glacial classification in monsoon areas. Quat Int, 2002, 97/98: 147–153
54 Yao T D, Thompson L G, Shi Y F, et al. Climate variation since the Last Interglaciation recorded in the Guliya ice core. Sci China Ser D-Earth Sci, 1997, 40: 662–668
55 Shi Y F, Yao T D. MIS3b (54–44 ka BP) cold period and glacial advance in middle and low latitudes (in Chinese). J Glaciol Geocryol, 2002, 24: 1–9
56 Wu J L, Wang S M, Shi Y F, et al. Temperature estimation by oxygen-stable record over the past 200 ka in Zogê basin. Sci China Ser D-Earth Sci, 2000, 43: 577–586
57 Wu J L, Wang S M, Pan H X, et al. Climatic variations in the past 140 ka recorded in core RM, east Qinghai-Xizang Plateau. Sci China Ser D-Earth Sci, 1997, 40: 443–448
58 Zhang H C, Wünnemann B, Ma Y Z, et al. Lake level and climate changes between 42000 and 18000 ^{14}C yr BP in the Tengger Desert, Northwestern China. Quat Res, 2002, 58: 62–72
59 Herzschuh U. Palaeo-moisture evolution in monsoonal Central Asia during the last 50000 years. Quat Sci Rev, 2006, 25: 163–178
60 Tang L Y, Shen C M, Liao G B, et al. Climatic changes in southeastern Tibet since LGM. Sci China Ser D-Earth Sci, 2004, 47: 436–442
61 Lisiecki L E, Raymo M E. A Pliocene-Pleistocene stack of 57 globally distributed benthic δ^{18}O records. Paleoceanography, 2005, 20: PA1003
62 Ziegler M. Orbital forcing of the late Pleistocene boreal summer monsoon: Links to North Atlantic cold events and the El Niño-Southern Oscillation. Dissertation for the Doctoral Degree. Utrecht: Utrecht University, 2009. 38–39
63 Lü R R, Zhao H L. Debris flow activity and environmental change on the eastern slope of Mt. Gongga during the Holocene (in Chinese). In: Chen F B, Luo J, eds. Ecological and Envirionmental Studies of High Mountain in the Mt. Gongga (Vol. 2). Beijing: China Meteorological Press, 1988. 90–101
64 Li C S. Problem on the water conservancy of the Moxi Platform, Luding, Xikang Province (in Chinese). Geol Rev, 1939, 4: 367–372